Study of GaN-Based Light-Emitting Diode (LED) With a Hybrid Surface Structure

Wei-Cheng Chen, Jing-Shiuan Niu, I-Ping Liu, Yu-Lin Lee, Shiou-Ying Cheng, *Member, IEEE*, Der-Feng Guo, and Wen-Chau Liu, *Senior Member, IEEE*

***Abstract*— A hybrid surface structure, incorporating an Ag-grid-based aluminum-doped zinc oxide (AZO) transparent conductive layer (TCL), a microhole array, 45°-sawtooth sidewalls, and an SiO_2 nanoparticle (NP)/microsphere (MS) passivation layer, is proposed for the characteristic improvement of GaN-based light-emitting diodes (LEDs). In order to optimize the contact behavior between the AZO and p-GaN layers, a 2-D Ag grid is applied on the contact interface. Because series resistance R_s is reduced by the conductive Ag-grid pattern, a lower forward voltage and a better current spreading ability are obtained. Compared with a conventional GaN LED with an injection current of 200 mA, the proposed device exhibits a forward voltage of 4.01 V, reduced from 4.34 V, and presents 33%, 34.4%, 45.4%, 33.1%, and 45.3% enhancements in the light output power (LOP), luminous flux, luminous efficacy, external quantum efficiency (EQE), and wall-plug efficiency (WPE), respectively. Moreover, a more effective current spreading in the light emission mapping image and a higher intensity in the far-field pattern are achieved. Improvements of both electrical and optical properties verify that the proposed device is promising for practical applications in solid-state lighting.**

***Index Terms*— 45°-sawtooth sidewall, Ag grid, current spreading, GaN, hybrid surface structure, light-emitting diodes (LEDs), microhole array, SiO_2 nanoparticle (NP)/microsphere (MS), transparent conductive layer (TCL).**

I. Introduction

GaN-BASED light-emitting diodes (LEDs) have been widely applied in outdoor full-color displays, monitor backlighting, and traffic lights due to the wide direct bandgap and excellent thermal performance of GaN material [1]–[4]. However, resulting from the large difference in the refractive index between GaN ($n = 2.5$) and the surrounding air ($n = 1$), the critical angle of total internal reflection (TIR) is around 23.5°, which only allows about 4% of the generated light in the GaN LEDs to escape into free space [5], [6]. In previous works, microhole arrays and 45°-sawtooth sidewalls were used to increase the possibility of photons finding the escape cone to emit out of LED devices [7]. In addition, an SiO_2 nanoparticle (NP)/microsphere (MS) passivation layer was employed to further enhance the photons scattered into the free space [8]. Furthermore, the current crowding, which leads to localized overheating and thermal hot spots, is another limiting factor to GaN LEDs used for practical applications in solid-state lighting. With the inherent properties of a wide bandgap, low resistivity, high transmittance, low cost, nontoxicity, and good thermal stability, aluminum-doped zinc oxide (AZO) has, therefore, been recognized as a candidate for transparent conductive layers (TCLs) [9]–[11]. However, the AZO/p-GaN interface does not offer the expected Ohmic contact [9], [12], [13]. To overcome this problem, many approaches, such as AZO/indium tin oxide (ITO) bilayer films [14], [15], AZO/Ni and AZO/NiO contact layers [16], and AZO/metal-based TCLs [17], have been proposed. In this article, a new hybrid surface structure, including an Ag-grid-based AZO TCL, a microhole array, 45°-sawtooth sidewalls [18], and an SiO_2 NP/MS passivation layer, is proposed to lower the forward voltage, increase the light extraction, and improve the current spreading of GaN-based LEDs. As series resistance R_s is reduced by the Ag-grid-based AZO TCL, the proposed device presents a lower forward voltage and a better current spreading ability than a conventional GaN LED. Besides, the proposed device exhibits enhancements in the light output power (LOP), luminous flux, luminous efficacy, external quantum efficiency (EQE), and wall-plug efficiency (WPE) due to the employment of the microhole array, 45°-sawtooth sidewalls, and SiO_2 NP/MS passivation layer to increase the photons emitting out of device.

Manuscript received July 16, 2020; revised September 2, 2020; accepted September 10, 2020. Date of publication October 6, 2020; date of current version October 22, 2020. This work was supported in part by the Ministry of Science and Technology under Contract MOST 109-2221-E-006-083-MY2. The review of this article was arranged by Editor J. D. Phillips. *(Corresponding authors: Der-Feng Guo; Wen-Chau Liu.)*

Wei-Cheng Chen, Jing-Shiuan Niu, Yu-Lin Lee, and Wen-Chau Liu are with the Department of Electrical Engineering, Institute of Microelectronics, National Cheng Kung University, Tainan 70101, Taiwan (e-mail: wcliu@ncku.edu.tw).

I-Ping Liu is with the Department of Material Technology, Green Technology Research Institute, CPC Corporation, Kaohsiung City 81126, Taiwan.

Shiou-Ying Cheng is with the Department of Electrical Engineering, National Ilan University, Yilan 26047, Taiwan.

Der-Feng Guo is with the Department of Electronic Engineering, R.O.C. Air Force Academy, Kaohsiung City 820, Taiwan (e-mail: g6f6guo@ms5.hinet.net).

Color versions of one or more of the figures in this article are available online at http://ieeexplore.ieee.org.

Digital Object Identifier 10.1109/TED.2020.3025844

II. Experiment

The fabrication flowchart of the proposed device is shown in Fig. 1. The device structure was grown on a sapphire substrate by a metal–organic chemical vapor deposition system. The epitaxial layers included a 2-μm-thick undoped GaN layer, a 2-μm-thick Si-doped n-GaN layer ($n = 1 \times 10^{18}$ cm^{-3}), 15-period InGaN/GaN multiple quantum wells (MQWs) as active layers, and a 0.3-μm-thick Mg-doped p-GaN layer ($p = 4 \times 10^{17}$ cm^{-3}), as shown in Fig. 1(a). After epitaxial growth and wafer cleaning, a photoresist layer was deposited

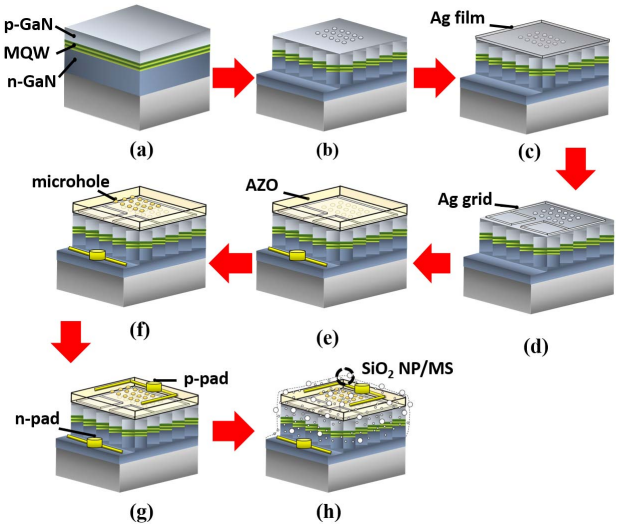

Fig. 1. Fabrication flowchart of the proposed GaN-based LED (a) the typical GaN-based LED structure after epitaxial growth, (b) mesa etching with 45°-sawtooth sidewalls and microhole array by ICP, (c) Ag thin film deposited by VTE, (d) formation of Ag grids, (e) formation of AZO TCL by RF sputtering, (f) formation of microhole array by wet etching process, (g) formation of p- and n-pad by VTE approach, and (h) formation of SiO_2 NP/MS passivation by RCD process.

on the top surface of the p-GaN layer, and a photolithography process was employed to define the patterns of the microhole array and 45°-sawtooth sidewalls [18]. The diameter of the microholes was 7-μm and the side length of each 45°-sawtooth sidewall was 10-μm [18]. The patterns were then transferred into the device structure with a depth of 1.2-μm by Cl_2/BCl_3 (20/10 sccm, 2 Pa) inductively coupled plasma (ICP) for 135 s under a source power of 300 W, as shown in Fig. 1(b). A 5-nm-thick Ag film was deposited by vacuum thermal evaporation (VTE), as shown in Fig. 1(c). Photolithography and etching processes were used to establish an Ag-grid pattern, as shown in Fig. 1(d). A geometric design of the Ag-grid pattern is shown in Fig. 2. The spacing lengths L_1–L_5 of Ag strips are $L_1 = 510$ μm and L_2–$L_5 = 210$ μm. The width of each Ag strip is 10 μm. Then, a 500-nm-thick AZO was deposited by radio frequency (RF) sputtering, as shown in Fig. 1(e). The photolithography process and $HCl:FeCl_3:H_2O$ = 1:1:1 etching solution were used to form microholes through the AZO layer to the substrate, as shown in Fig. 1(f). The AZO layer was annealed in an N_2 ambience at 800 °C for 3 min by a rapid thermal annealing (RTA) system. Cr/Pt/Au (25/50/2000 nm) metals were sequentially deposited by the VTE approach and defined as n- and p-electrode pads by lift-off process, as shown in Fig. 1(g). The n-and p-electrode pads were activated in an N_2 ambience at 400 °C for 10 min to improve the metal–semiconductor (MS) contact properties. The effective area of p-electrode was 5.59×10^{-4} cm^2. The SiO_2 NP/MS passivation layer was coated by a rapid convective deposition (RCD) approach [8]. This passivation layer was formed with an SiO_2 NP:SiO_2 MS:sodium dodecyl sulfate (SDS):ethanol:de-ionized (DI) water = 1:1:10:10:10 solution [8]. Finally, the SiO_2 NP/MS passivation layer above the n- and p-electrode pads was removed with a buffer oxide etching (BOE) solution, as shown in Fig. 1(h).

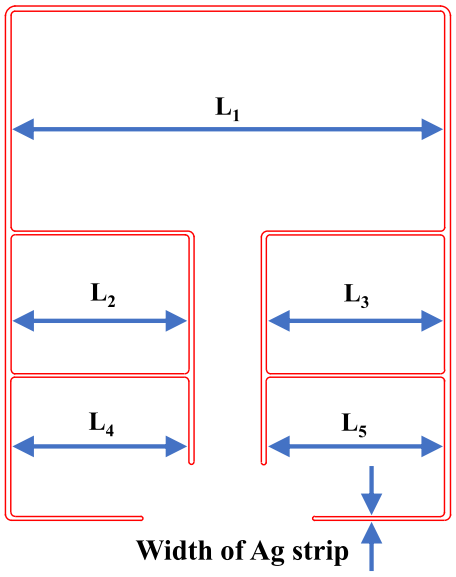

Fig. 2. Geometric design of the Ag-grid pattern.

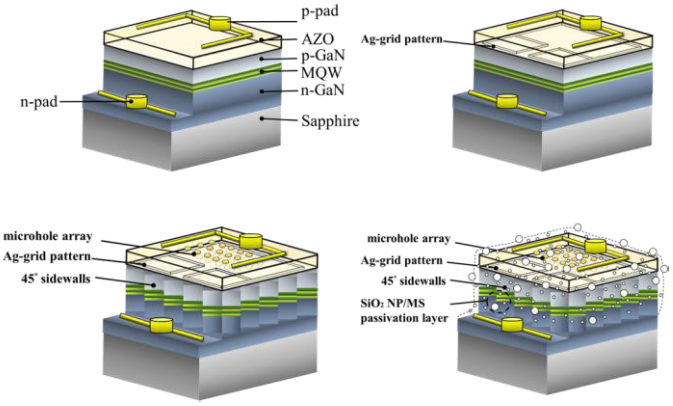

Fig. 3. Schematic cross-sectional diagrams of the studied devices A–D.

For comparisons, a conventional GaN LED (denoted as Device A), a GaN LED with a 2-D Ag grid (denoted as Device B), a GaN LED with a 2-D Ag grid, a microhole array, and 45°-sawtooth sidewalls (denoted as Device C), and a GaN LED with a 2-D Ag grid, a microhole array, 45°-sawtooth sidewalls, and a SiO_2 NP/MS passivation layer (denoted as Device D) were fabricated. Schematic cross-sectional diagrams of Devices A–D are depicted in Fig. 3. To reduce the process deviation, all studied devices were fabricated from the same LED wafer. All the studied devices were diced into 650 × 550-μm^2 chips. The chips were then attached and bonded to TO-3 submounts for the electrical and optical tests. Properties of the fabricated devices were measured by a semiconductor parameter analyzer (HP-4155C) and an integrated sphere system (ISP-150, C&M Tech. Corporation).

III. Results and Discussion

Fig. 4(a) and (b) shows the top-view scanning electron microscopy (SEM) images of Device A and Device C, and Fig. 4(c) and (d) shows the corresponding enlarged views, respectively. The Ag-grid pattern is almost transparent,

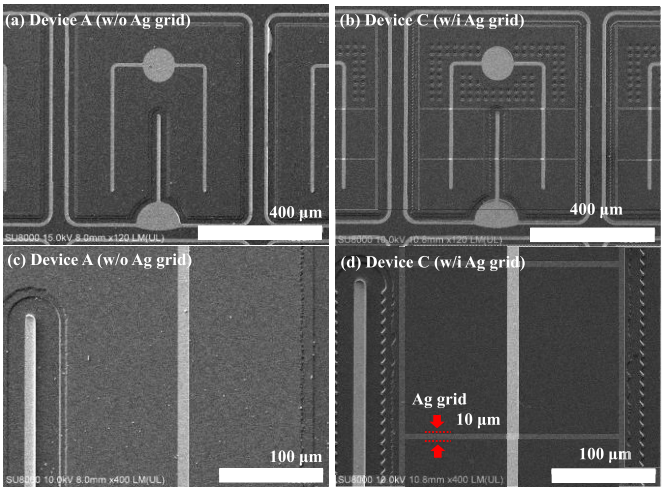

Fig. 4. Top-view SEM images of (a) Device A and (b) Device C and enlarged views of (c) Device A and (d) Device C.

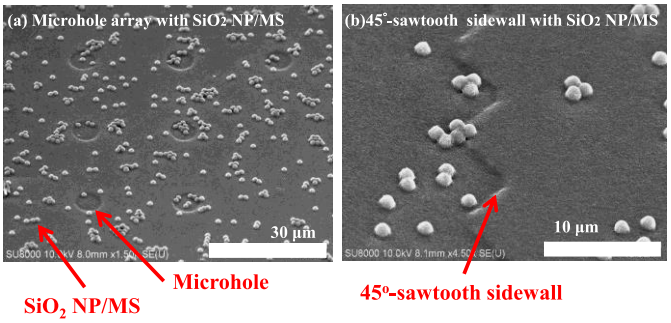

Fig. 5. Tilt-view SEM images of the SiO_2 NP/MS passivation layer around the (a) microhole array and the (b) 45°-sawtooth sidewall of Device D.

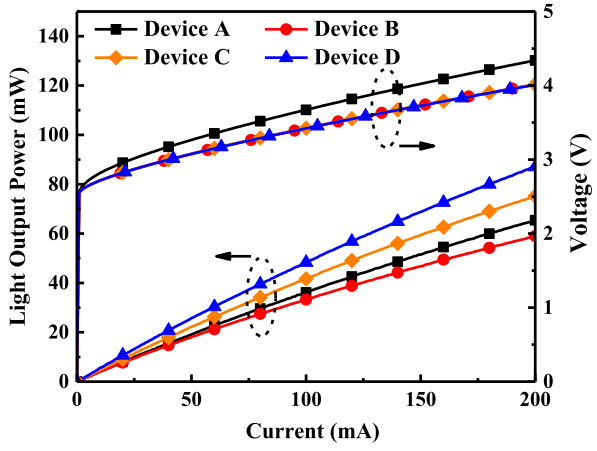

Fig. 6. L–V–I characteristics of the studied devices A–D.

as shown in Fig. 4(b) and (d), due to its extreme thinness of only 5 nm. The width of each metal strip is 10-μm. The transparent design of the Ag-grid pattern could enhance the photons to penetrate the Ag grid rather than being absorbed. Fig. 5(a) and (b) shows tilt-view SEM images of the SiO_2 NP/MS passivation layer around the microhole array and the 45°-sawtooth sidewall of Device D.

Fig. 6 shows the LOP–voltage–current (L–V–I) characteristics of the studied devices. The forward voltages of Devices A–D at an injection current of 200 mA are 4.34, 4.01, 4.01, and 4.01 V, respectively. Relatively low forward voltages of Devices B–D are obtained, which are expected because the Ag-grid-based AZO film provides better contact conductivity and current spreading than AZO directly deposited on the p-GaN surface. Fig. 7 shows the reverse-biased I–V curves of the studied devices. Leakage currents of Devices A–D at a reverse-biased voltage of −5 V are 13.2 (2.06), 13.3 (2.07), 13.4 (2.08), and 1.64 (0.26) nA (μA/cm^2), respectively. The relatively low reverse leakage current of Device D results from the SiO_2 NP/MS passivation layer providing a better insulation property. In addition, the series resistance R_s can be estimated by [7]

$$I\left(\frac{dV}{dI}\right) = IR_s + \eta\frac{KT}{q} \tag{1}$$

where η, K, T, and q are the ideality factor, Boltzmann's constant, absolute temperature, and electronic charge, respectively. Fig. 8 shows $I(dV/dI)$ and dynamic resistance R_D as a function of the injection current. The R_s values of Devices A–D are 8.34 (1.3), 7.18 (1.12), 7.18 (1.12),

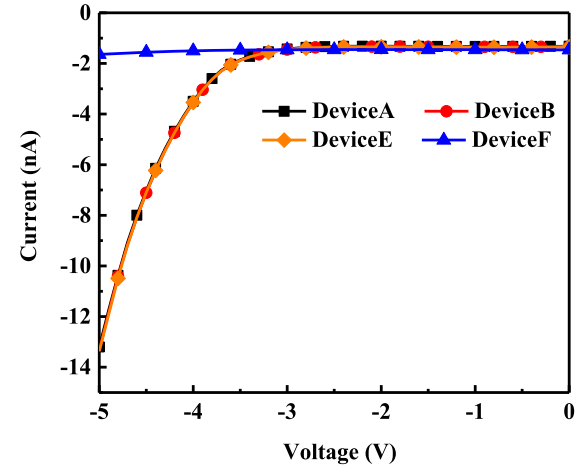

Fig. 7. Reverse-biased current–voltage (I–V) curves of the studied devices A–D.

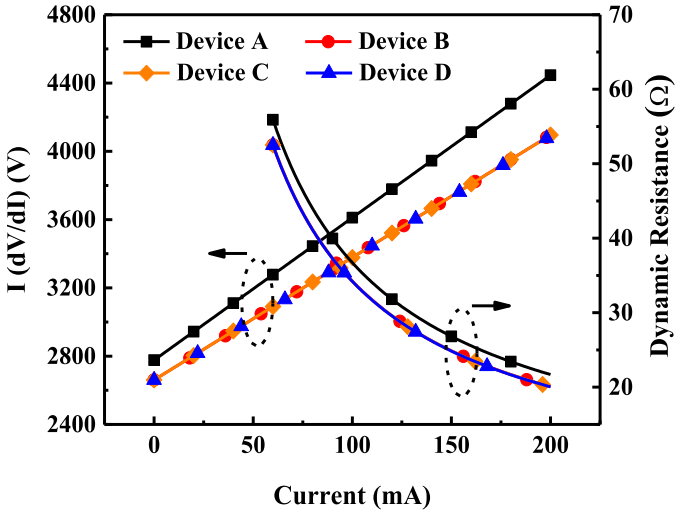

Fig. 8. $I(dV/dI)$ and dynamic resistance R_D as a function of the injection currents of the studied devices A–D.

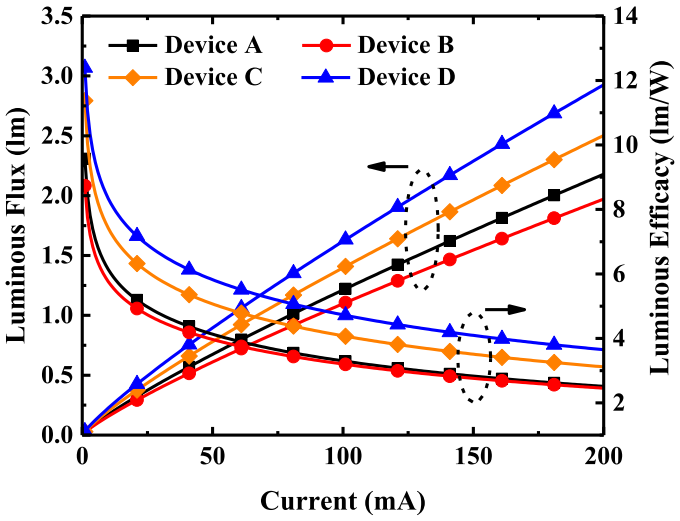

Fig. 9. Luminous flux and luminous efficacy as a function of the injection currents of the studied devices A–D.

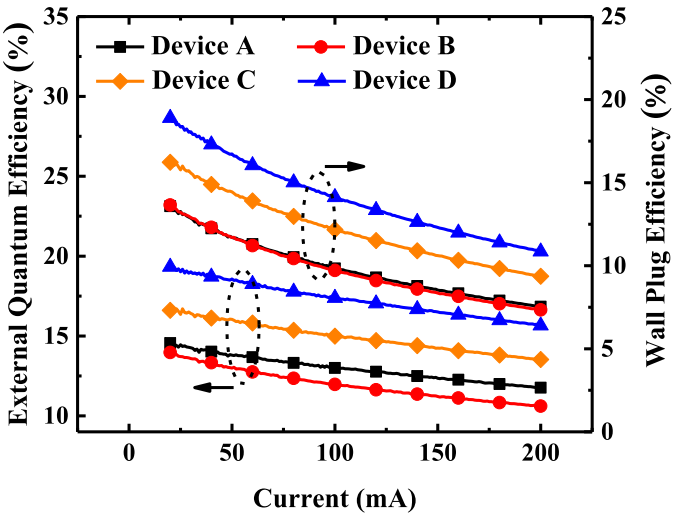

Fig. 10. WPE and EQE as a function of the injection currents of the studied devices A–D.

and 7.15 (1.11) Ω (kΩ/cm^2), respectively. The R_D values of Devices A–D at 200 mA are 21.7 (38.8), 20.07 (35.9), 20.07 (35.9), and 20.04 (35.8) Ω (kΩ/cm^2), respectively. Compared with Device A, Devices B–D present lower R_s and R_D values due to the improved electrical performance the Ag grid. The LOP values of Devices A–D at 200 mA are 65.4, 59, 75.2, and 87 mW, respectively, as shown in Fig. 6. Compared with Device A, Devices B–D show LOP increments of −9.8%, 14.9%, and 33%, respectively. Device B exhibits a lower output power than Device A. This negative increment is attributed to the fact that the Ag grid causes an absorption effect of emitting photons [19]. Although a transparent design of the Ag ultrathin layer was utilized on the studied devices, the light absorption of metal film still could not completely be avoided. To enhance the optical performance, a microhole array, 45°-sawtooth sidewalls, and a SiO_2 NP/MS passivation layer were employed in the structures of Devices C and D. The LOP values of Devices C and D show obvious positive increments. The microhole array and patterned sidewalls can effectively reduce the effect of TIR and increase the escape opportunity of lights generated inside devices [7]. Moreover, the SiO_2 NP/MS passivation layer can provide a rough surface and antireflective characteristics to further scatter and redirect photons into free space [8].

Fig. 9 shows the luminous flux and luminous efficacy as a function of the injection current of the studied devices. At 200 mA, Devices A–D present luminous fluxes of 2.18, 1.97, 2.5, and 2.93 lm, and luminous efficacies of 2.51, 2.45, 3.12, and 3.65 lm/W, respectively. Compared with Device A, Devices B–D show −9.6%, 14.7%, and 34.4% increments in luminous fluxes and −2.4%, 24.3%, and 45.4% increments in luminous efficacies, respectively. The luminous flux increments of Devices B–D show almost similar values to the LOP increments mentioned above, which confirms that the degradation of optical performance, resulting from light absorption by the Ag grid, can compensate for with the usage of the proposed hybrid structure. Devices B–D exhibit

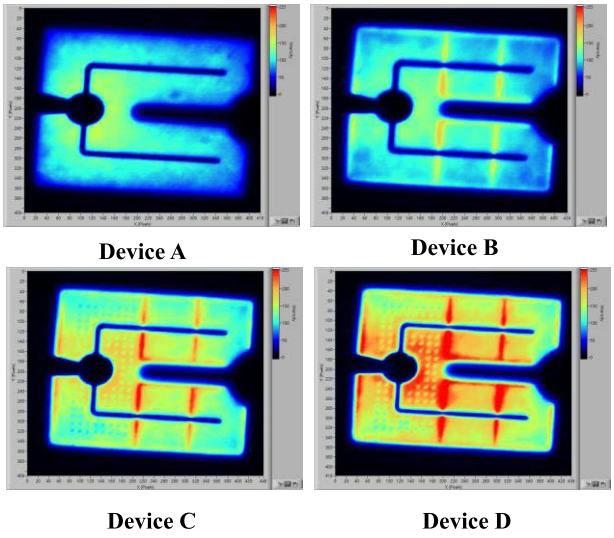

Fig. 11. Light emission mapping images at 100-mA injection current of the studied devices A–D.

better improvements in luminous efficacy than in luminous flux under the same injection current. This result implies that the conversion from electrical to optical energy is effectively improved by the Ag grid that causes a lower forward voltage and better light extraction.

Fig. 10 shows the characteristics of WPE and EQE as a function of the injection currents of Devices A–D. At 200 mA, the WPE values of Devices A–D are 7.5%, 7.3%, 9.4%, and 10.9%, and the EQE values are 11.8%, 10.6%, 13.5%, and 15.7%, respectively. Compared with Device A, Devices B–D show −2.7%, 25.3%, and 45.3% increments in the WPE values, and −10.2%, 14.4%, and 33.1% increments in the EQE values, respectively. WPE is an energy conversion efficiency from electrical power into optical power [20]. The Ag-grid-based AZO can contribute improvements in the electrical characteristics of the studied devices, including turn-on voltages, series resistances, and dynamic resistances. Thus, Devices

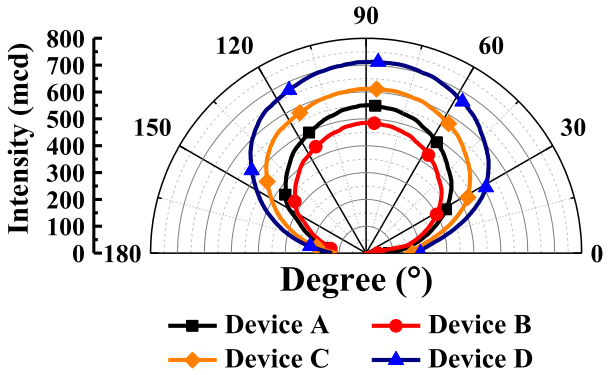

Fig. 12. Far-field radiation patterns of the studied devices A–D.

B–D can retain good optical and electrical performances. In addition, the EQE characteristics verify that the microhole array, 45°-sawtooth sidewall, and SiO_2 NP/MS passivation layer can further enhance the light output performance, even if there is an unavoidable absorption effect from the Ag grid.

Fig. 11 shows the light emission mapping images of Devices A–D at an injection current of 100 mA. Compared with Device A, Devices B–D show better current spreading, which is attributed to the fact that the conductive Ag-grid pattern guides the injection current to the entire emission region instead of around the p-electrodes. Far-field radiation patterns of Devices A–D are shown in Fig. 12. The corresponding divergent angles (angle of half-maximum emission intensity) of Devices A–D are 133°, 133°, 141°, and 145°, respectively. Device D exhibits the highest light intensity and the widest divergent angle in the omnidirectional radiation, which implies that photons can be further effectively scattered and extracted into the free space due to the usage of the microhole array, 45°-sawtooth sidewall, and SiO_2 NP/MS passivation layer.

IV. Conclusion

A hybrid surface structure, incorporating an Ag-grid-based AZO TCL, a microhole array, 45°-sawtooth sidewalls, and an SiO_2 NP/MS passivation layer, is proposed to fabricate GaN LEDs. Compared with a conventional GaN LED, the proposed device exhibits a lower forward voltage and presents enhancements in LOP, luminous flux, luminous efficacy, EQE, and WPE. A uniform current spreading in the light emission mapping image and a higher intensity in the far-field pattern are also obtained. Thus, the hybrid structure is promising for use in fabricating high-performance GaN LEDs for applications in the solid-state lighting area.

Acknowledgment

The technical assistance on SEM operation by Hui-Jung Shih (Instrument Center, National Cheng Kung University, Taiwan) is appreciated.

References

[1] T. Mukai, M. Yamada, and S. Nakamura, "Characteristics of InGaN-based UV/blue/green/amber/red light-emitting diodes," *Jpn. J. Appl. Phys.*, vol. 38, pp. 3976–3981, Jul. 1999, doi: 10.1143/JJAP.38.3976.

[2] M. Koike, N. Shibata, H. Kato, and Y. Takahashi, "Development of high efficiency GaN-based multiquantum-well light-emitting diodes and their applications," *IEEE J. Sel. Topics Quantum Electron.*, vol. 8, no. 2, pp. 271–277, Mar./Apr. 2002, doi: 10.1109/2944.999180.

[3] J. Zhu, H. Zhang, Z. Zhu, Q. Li, and G. Jin, "Surface-plasmon-enhanced GaN-LED based on the multilayered rectangular nano-grating," *Opt. Commun.*, vol. 322, pp. 66–72, Jul. 2014, doi: 10.1016/j.optcom.2014.02.011.

[4] Y.-C. Chang, J.-K. Liou, and W.-C. Liu, "Improved light extraction efficiency of a high-power GaN-based light-emitting diode with a three-dimensional-photonic crystal (3-D-PhC) backside reflector," *IEEE Electron Device Lett.*, vol. 34, no. 6, pp. 777–779, Jun. 2013, doi: 10.1109/LED.2013.2255020.

[5] P. Mao *et al.*, "Extraction of light trapped due to total internal reflection using porous high refractive index nanoparticle films," *Nanoscale*, vol. 6, no. 14, pp. 8177–8184, 2014, doi: 10.1039/C4NR01065E.

[6] B.-U. Ye *et al.*, "Enhancing light emission of nanostructured vertical light-emitting diodes by minimizing total internal reflection," *Adv. Funct. Mater.*, vol. 22, no. 3, pp. 632–639, Feb. 2012, doi: 10.1002/adfm.201101987.

[7] Y.-L. Lee and W.-C. Liu, "Enhanced light extraction of GaN-based light-emitting diodes with a hybrid structure incorporating microhole arrays and textured sidewalls," *IEEE Trans. Electron Devices*, vol. 65, no. 8, pp. 3305–3310, Aug. 2018, doi: 10.1109/TED.2018.2849353.

[8] C.-H. Chang, Y.-L. Lee, Z.-F. Wang, R.-C. Liu, J.-H. Tsai, and W.-C. Liu, "Performance improvement of GaN-based light-emitting diodes with a microhole array, 45° sidewalls, and a SiO_2 nanoparticle/microsphere passivation layer," *IEEE Trans. Electron Devices*, vol. 66, no. 1, pp. 505–511, Jan. 2019, doi: 10.1109/TED.2018.2882802.

[9] B.-R. Huang, C.-C. Liao, W.-C. Ke, Y.-C. Chang, H.-P. Huang, and N.-C. Chen, "Poole-frenkel effect on electrical characterization of Al-doped ZnO films deposited on p-type GaN," *J. Appl. Phys.*, vol. 115, no. 11, Mar. 2014, Art. no. 113705, doi: 10.1063/1.4869137.

[10] J.-K. Liou, C.-C. Chen, P.-C. Chou, T.-Y. Tsai, S.-Y. Cheng, and W.-C. Liu, "Improved current spreading performance of a GaN-based light-emitting diode with a stair-like ITO layer," *Solid-State Electron.*, vol. 99, pp. 21–24, Sep. 2014, doi: 10.1016/j.sse.2014.05.002.

[11] H. K. Lee, D. H. Joo, Y. H. Ko, Y. Yeh, Y. P. Kim, and J. S. Yu, "Improved light extraction of GaN-based blue light-emitting diodes with ZnO nanorods on transparent Ni/Al-doped ZnO current spreading layer," *Jpn. J. Appl. Phys.*, vol. 51, Nov. 2012, Art. no. 122102, doi: 10.1143/JJAP.51.122102.

[12] C. H. Kuo *et al.*, "Low operation voltage of nitride-based LEDs with Al-doped ZnO transparent contact layer," *Electrochem. Solid-State Lett.*, vol. 11, no. 9, p. H269, 2008, doi: 10.1149/1.2953680.

[13] J.-K. Sheu, Y. S. Lu, M.-L. Lee, W. C. Lai, C. H. Kuo, and C.-J. Tun, "Enhanced efficiency of GaN-based light-emitting diodes with periodic textured Ga-doped ZnO transparent contact layer," *Appl. Phys. Lett.*, vol. 90, no. 26, Jun. 2007, Art. no. 263511, doi: 10.1063/1.2753110.

[14] S. L. Ou, D. S. Wuu, S. P. Liu, Y. C. Fu, S. C. Huang, and R. H. Horng, "Pulsed laser deposition of ITO/AZO transparent contact layers for GaN LED applications," *Opt. Express*, vol. 19, no. 17, pp. 16244–16251, 2011, doi: 10.1364/OE.19.016244.

[15] D. Chen, J. Lu, R. Lu, L. Chen, and Z. Ye, "High-performance GaN-based LEDs with AZO/ITO thin films as transparent contact layers," *IEEE Trans. Electron Devices*, vol. 64, no. 6, pp. 2549–2555, Jun. 2017, doi: 10.1109/TED.2017.2693499.

[16] C. J. Tun *et al.*, "Applications of transparent Al-doped ZnO contact on GaN-based power LED," *Proc. SPIE*, vol. 61210, Mar. 2006, Art. no. 61210X, doi: 10.1117/12.647123.

[17] C.-H. Hsu *et al.*, "Study of a GaN-based LED with an Al/AZO composite transparent conductive layer," *IEEE Trans. Electron Devices*, vol. 64, no. 9, pp. 3678–3682, Sep. 2017, doi: 10.1109/TED.2017.2724599.

[18] C. Y. Chen and W.-C. Liu, "Light extraction enhancement of GaN-based light-emitting diodes with textured sidewalls and ICP-transferred nanohemispherical backside reflector," *IEEE Trans. Electron Devices*, vol. 64, no. 9, pp. 3672–3677, Sep. 2017, doi: 10.1109/TED.2017.2720685.

[19] C.-S. Hsu *et al.*, "Performance enhancement of GaN-based light-emitting diodes by using transparent Ag metal line patterns," *IEEE Trans. Electron Devices*, vol. 64, no. 6, pp. 2542–2548, Jun. 2017, doi: 10.1109/TED.2017.2691411.

[20] J. H. Son *et al.*, "Enhancement of wall-plug efficiency in vertical InGaN/GaN LEDs by improved current spreading," *Opt. Express*, vol. 20, no. 2, p. A287, Mar. 2012, doi: 10.1364/OE.20.00A287.